Supplemental Figures

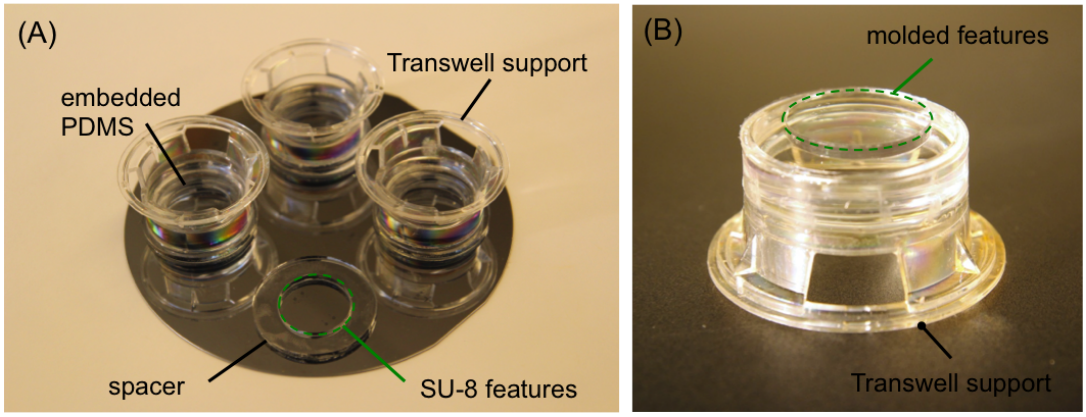

Fig. S1 Embedding of microchannel layer in plastic supports. (A) Plastic transwell supports modified with a coating of vinyl/APTES silane are placed on spacers to embed a thick micromolded PDMS layer. (B) After curing for 48 hours at room temperature, the layer is removed from the wafer. The 'molded features' extend an additional 1.8 mm beyond the edge of the Transwell support in order to define a 250 µm gap between the final device and the cover-glass of the 6-well plate.

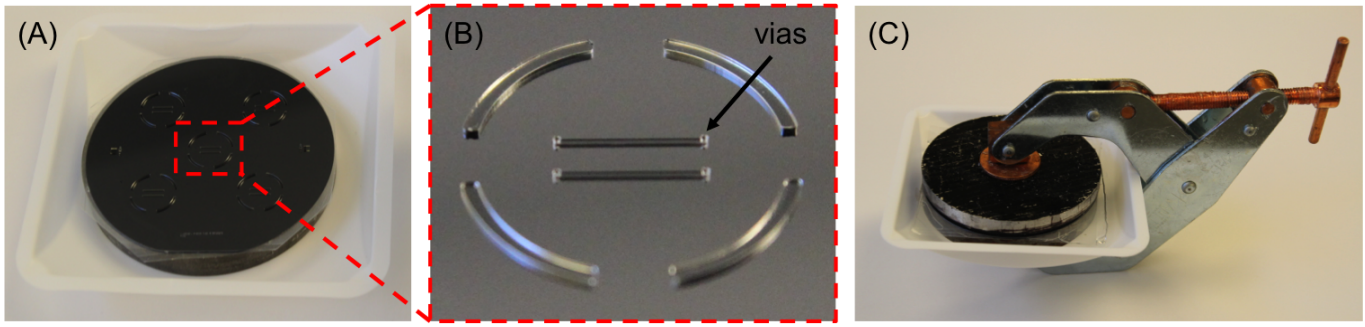

Fig. S2 Exclusion molding of thin PDMS layers. (A) Photograph of the SU-8 photopatterned silicon wafer. (B) Enlarged view of a single mold. The circular boundary perforates the layer to assist de-molding. (C) The complete exclusion molding assembly. The large weigh boat catches the uncured PDMS that is displaced during clamping.

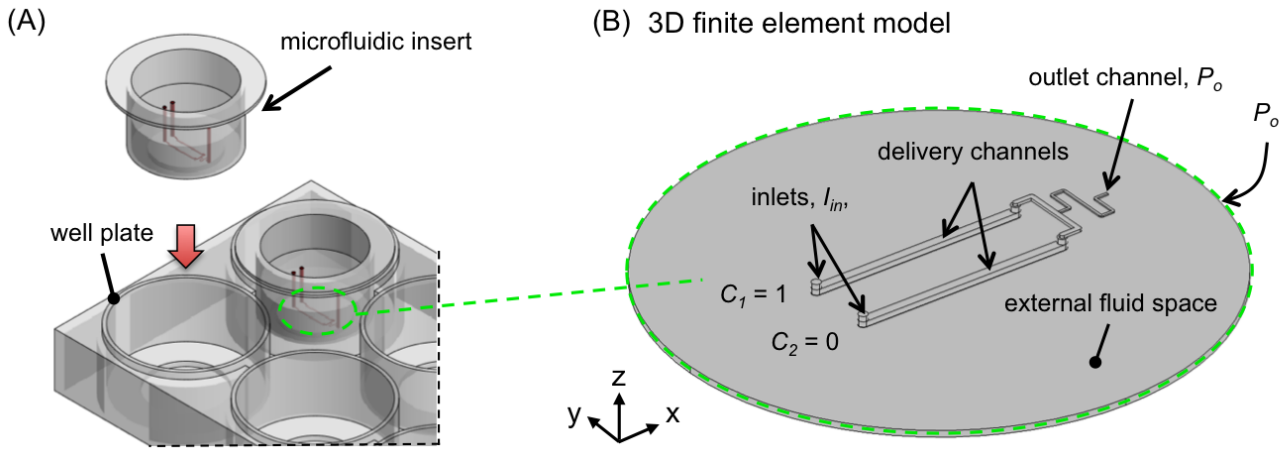

Fig. S3 Contextual diagram of the simulated region and FEM geometry. (a) The model represents the fluid flow of the device microchannel network and the external fluid space between the membrane and the cell culture surface of the 6-well plate. (b) The boundary conditions for the simulation assume defined inlet flows I_m with normalized concentrations of $C_1 = 1$ and $C_2 = 0$. The edge of the fluid space and the outlets microchannels are set to Po = 0 and open for convective flux of the transported species. Walls are defined with a no slip condition. Separating the gradient channels and the fluid space is a 12 µm thin domain of the same area that defines the track-etched membrane flows using the permeability parameter, $k = 3.927 \times 10^{-16}$ m^2.

Tracking of neutrophil migration and chemotaxis

Time lapse images of HL-60s underneath microfluidic transwell gradients were collected at 30 second intervals using a Nikon TE-Eclipse as described earlier. Automated large-area image stitching was used to generate a composite image of 24 fields of view with 15% overlap using the 10X objective for phase-contrast and epi-fluorescence (**Fig S4(a)**). Automated shading correction was enabled in the NIS-Elements software to correct for non-uniform illumination of both phase-contrast and fluorescence images. 12-bit tiff images were collected with a bin of 2 that were sufficient to resolve single cells as shown in **Fig. S4(b)**. Time-lapse image series of 1.5 hours in length were collected for experiments applying gradients of 100 nM fMLP and controls with either uniform 100 nM fMLP or no fMLP. Image processing and automated tracking of cell migration was accomplished with the FIJI package of Image J. First the phase-contrast tiff images were processed using edge detection to enhance local regions of sharp changes in intensity as shown in **Fig. S5(A-B)**. Next images were despeckled to remove small-diameter regions of high-intensity that result from background noise. Finally, a Gaussian filter is used to smooth the images and fill in the low intensity "hole" from the center of the cell bodies. The final result shown in **Fig. S5(C)** is dark image with intensity maxima located roughly where the cell center was located in the original images. The fluorescence images taken during live-time lapse experiments were used to verify the development of the fMLP gradient and equivalent flow conditions for the controls in which a tracer was still used (**Fig. S6**).

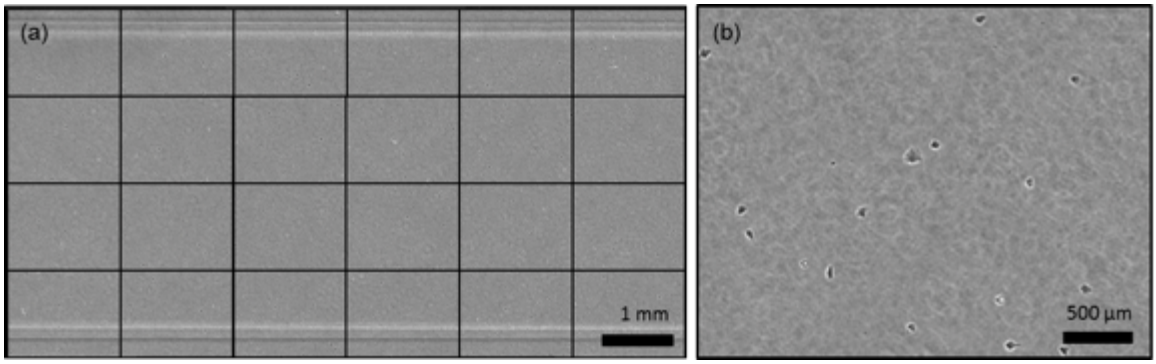

Fig. S4 Large-area image stitching for time lapse tracking of HL-60 migration during chemotaxis experiments. (a) A large-area stitched image was acquired every 25 seconds by capturing the composite of 24 individual fields of view using the motorized translation stage. (b) The cells are visible in phase-contrast for a single field of view captured using the 10X objective. High contrast, large-area imaging, and sufficient time resolution is essential for the automated tracking of individual migrating cells.

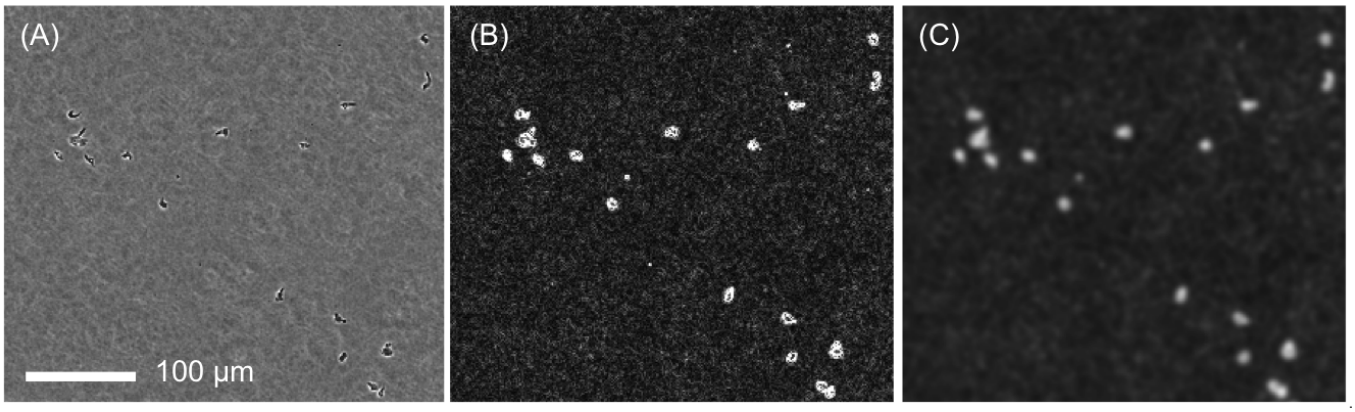

Fig. S5 Image processing for automated identification of cell bodies with Image J. (A) A cropped view of an original phase-contrast image taken at 10X. (B) The edge detected image that enhances sharp changes in contrast. (C) The despeckle filter is applied to remove small diameter and high intensity noise from the background, and a 4-pixel diameter Gaussian filter is applied to smooth the image and enhance identification of the cell bodies from high intensity regions.

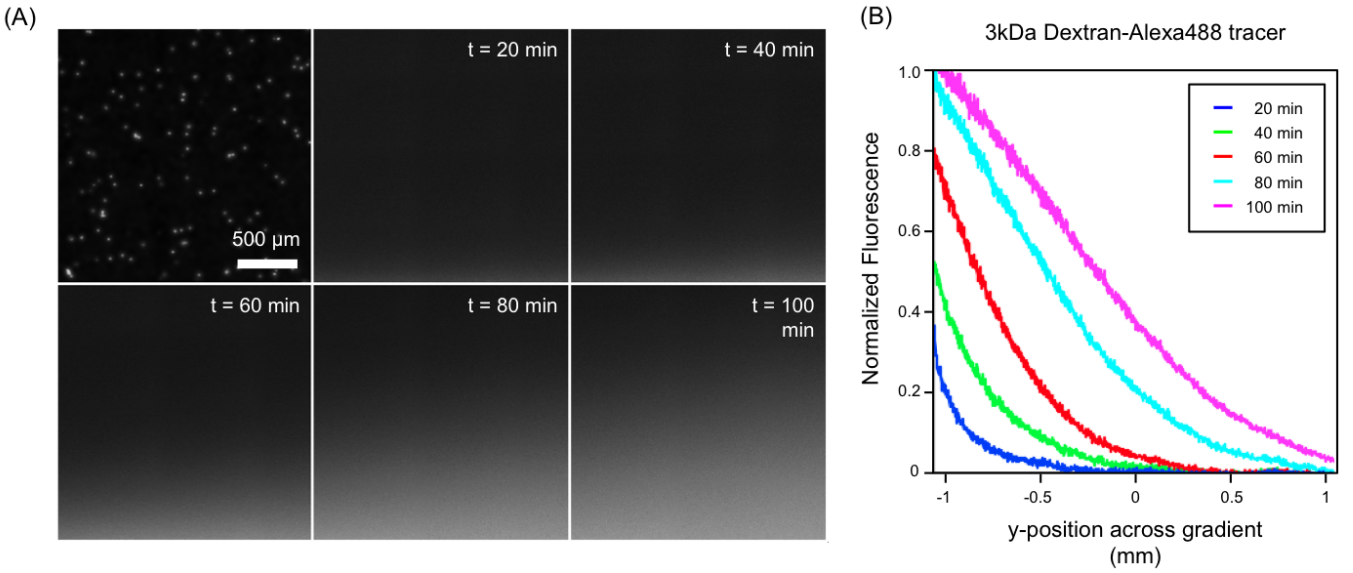

Fig. S6 Monitoring of the 100 nM fMLP gradient with a fluorescent tracer during time lapse of HL-60 chemotaxis. (a) A reference image showing the detected cells for a field of view spanning the length of the gradient and a time series of fluorescence images monitoring the 3 kDa Dextran-Alexa488 tracer. (b) The fluorescence intensity profiles corresponding to the time sequence demonstrate the evolution of the gradient.

Retinal explant cultures with growth factors

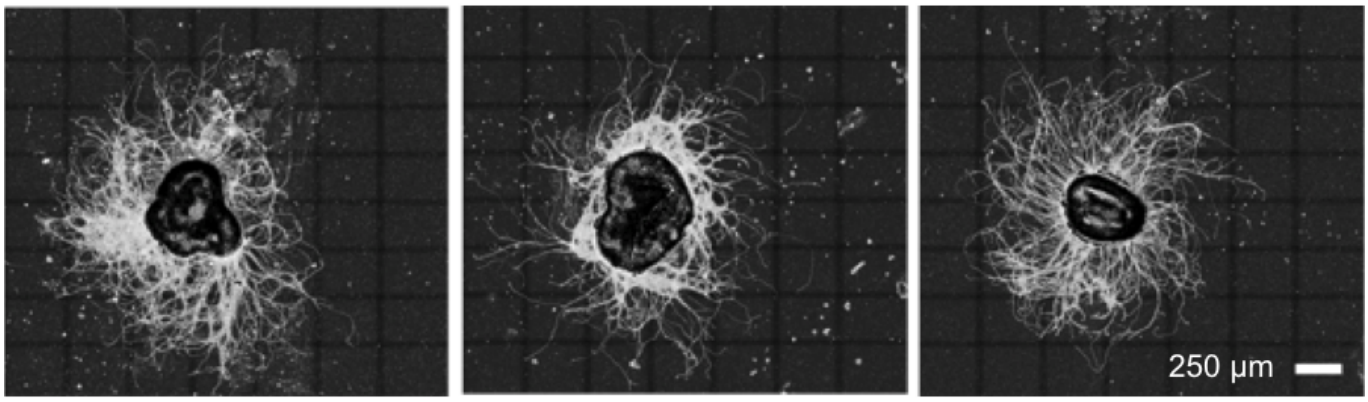

Fig. S7 E15 mouse retinal explants after 40 h cultured with BDNF and CNTF growth factors. Large-area stitched images are shown after edge detection to enhance neurite contrast.

Rotation of microfluidic transwell gradients

A feature of the modular design, the gradients can be altered rapidly by repositioning the device or removing the device altogether. In **Fig. S8** the device was repositioned at different angles by simply rotating the device relative to the original position in the 6-well plate.

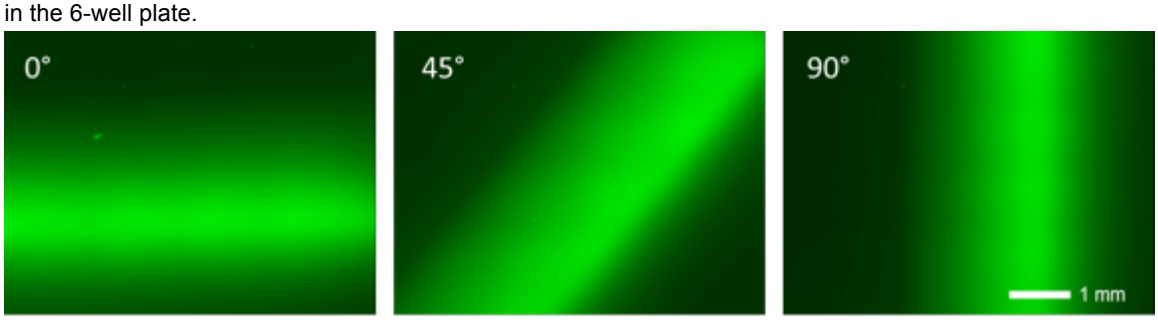

Fig. S8 Demonstration of tunable gradients through rotation of device. The series of surface-fluorescence images were taken at different rotational positions after allowing 30 min for the gradient to evolve using fluorescein and Orange G.

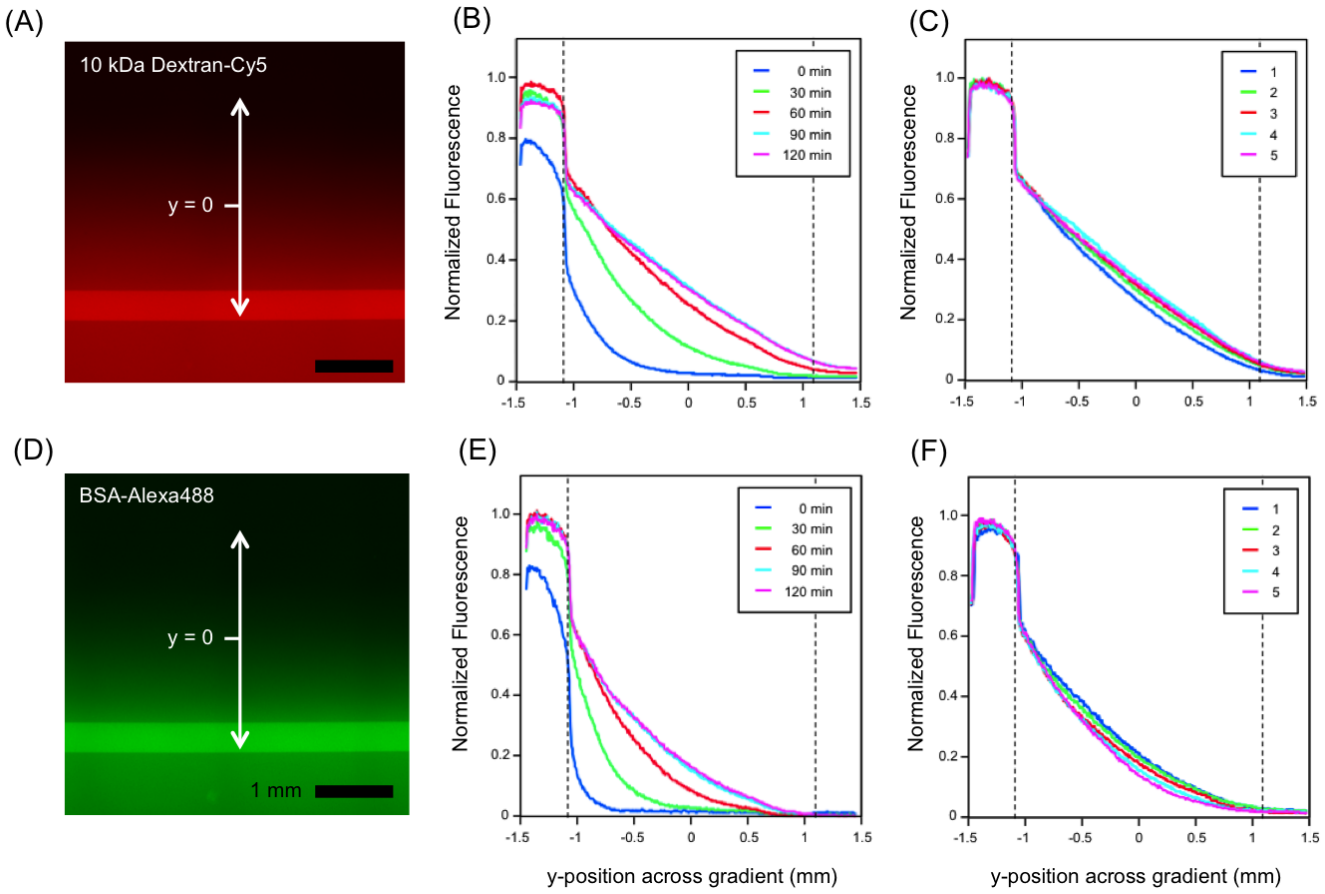

Fig. S9 Live-monitoring of microfluidic transwell gradients using fluorescent tracers. (A) A large-area stitched epi-fluorescence image taken after 24 hours with 5 μM 10 kDa dextran-Cy5 in the lower channel and the device operated at a flow rate of 50 μl/hr. (B) Fluorescence intensity profile across the gradient reaches steady state at approximately 90 min. (C) Gradient profiles are plotted for five positions taken at 2 mm increments along the length of the 8 mm delivery channel. Similarly, the gradients for a 5 μM BSA–Alexa488 conjugate show (D) steady state, (E) evolution in 90 min, and (F) lateral uniformity.